

Ultracold long-range van der Waals Rydberg trimers

Mateo Londoño* and Jesús Pérez-Ríos

Department of Physics and Astronomy, Stony Brook University, Stony Brook, NY 11794, USA

Vanessa C. Olaya-Agudelo and Felipe Herrera

Department of Physics, Universidad de Santiago de Chile, Santiago 9170124, Chile

(Dated: February 18, 2025)

Rydberg molecules, Rydberg-atom or Rydberg-molecule, are an essential ingredient of cold molecular sciences. However, due to the richness of Rydberg-neutral interactions, new kinds of Rydberg molecules and binding mechanisms are still to be discovered. In this work, we predict the existence of ultra-long-range van der Waals trimers in dilute atom-gas mixtures. These are bound states of a Rydberg atom and a diatomic polar molecule mediated by the long-range van der Waals interaction. This new binding mechanism gives rise to trimers with sizes between 5-500 nm and binding energies between 2 MHz and 0.2 kHz depending on the atomic principal quantum number n and orbital angular momentum L . We show that these molecules can be produced via two-photon photoassociation, with rates on the order of $(10^{-13} - 10^{-11}) \text{ cm}^3\text{s}^{-1}$ for temperatures in the range of $(0.5 \mu\text{K} - 10\mu\text{K})$, and discuss the feasibility of observing trimer resonances.

I. INTRODUCTION

Rydberg atoms play a pivotal role in several areas of atomic, molecular, and optical physics [1], such as the implementation of novel quantum information protocols [2], quantum simulation of many-body Hamiltonians [3], the study of impurity physics, non-linear quantum optics, and ultracold chemistry [4–6]. Many of these applications rely on controlling the exaggerated properties of Rydberg states in order to tailor the resulting interatomic forces. For instance, at high densities, Rydberg excitations present a rather unique lineshape as a consequence of the Rydberg electron-perturber atom interaction [7, 8], leading to the formation of ultralong-range Rydberg molecules [9–19], and possible polaron effects, considering the Rydberg atom as an impurity in a dense atomic reservoir. [20–22] Another key ingredient of atomic, molecular, and optical physics is cold molecules, an essential platform for exploring fundamental quantum phenomena. For instance, controlling interactions enables precise studies of quantum chemistry [6], novel quantum phases [23], and quantum information processing [24]. Their long-range interactions and tunable states make them ideal for simulating complex quantum systems and advancing quantum technology applications. Cold molecules are also suitable for creating hybrid-quantum systems to study atomic or charged impurity dynamics [25, 26].

In combination with cold molecules, Rydberg atoms offer a unique opportunity for studying exotic Rydberg molecules. For instance, a Rydberg excitation in a dense dipolar gas can lead to the formation of an ultra-long-range Rydberg molecule bound state via elastic collisions

of the Rydberg electron with the molecule [27, 28]. When the Rydberg excitation is induced in a molecule, it gives rise to the formation of Rydberg bimolecules, an ultra-long range Rydberg molecule in which a molecular ionic core is bound to a molecule (inside the Rydberg orbit) via the scattering of the Rydberg electron off the perturbing molecule. These exotic molecules show binding energies in the GHz regime and kilo-Debye permanent dipole moments [29]. A similar scenario has been proposed as a technique for sympathetic cooling of molecules [30].

In this work, we predict the existence of another type of formed long-range Rydberg trimer molecule when a Rydberg atom binds to a diatomic polar molecule via van der Waals interaction, in a regime where the molecular density is much lower than the density of Rydberg atoms so that at most one molecule resides within the Rydberg blockade radius r_B , as displayed in Fig. 1. The long-range van der Waals Rydberg trimer is formed by a two-photon photoassociation scheme from the ground state of the atom and the molecule. In this case, in analogy to the lineshape of Rydberg excitations in atomic gases [1], the two-photon photoassociation lineshape spectra will show traces of the existence of long-range van der Waals Rydberg trimers.

The Van der Waals interaction, responsible of the bonding in these new trimers, dominates when the Rydberg-molecule distance is larger than the Le-Roy Radius. In this sense, the predicted trimers are formed in a density regime that is complementary to previous reported ultralong-range Rydberg molecules, where the oscillatory Born-Oppenheimer potentials are formed below the Le-Roy radius [31]. From this we expect to have exotic Rydberg trimers either the molecule is inside or outside the Rydberg's electron orbital, with a particular transition in the bonding mechanism at the limit of the two regions.

* mateo.londoo@stonybrook.edu

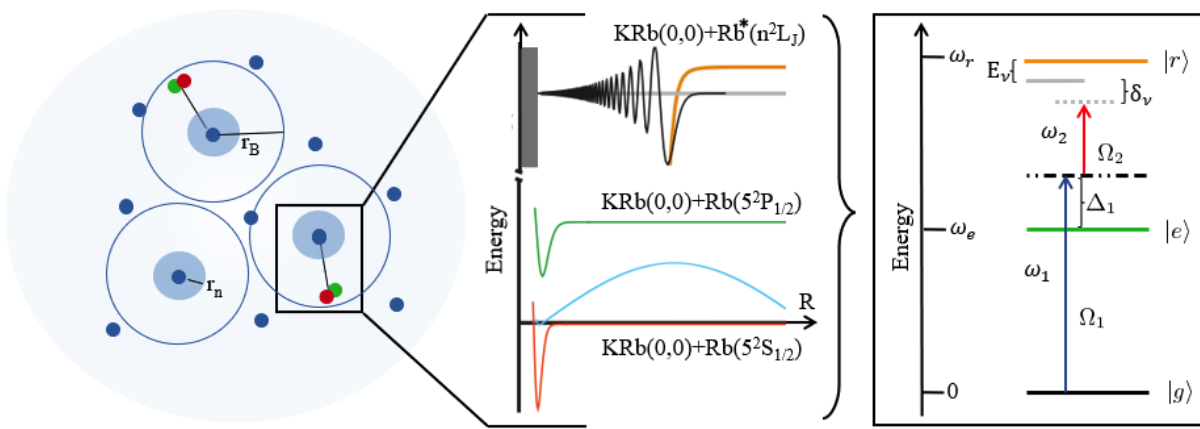
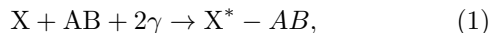


FIG. 1: **Formation of ultra-long range Rydberg trimers.** Left: Scheme of the atomic and molecular diluted gases, where not more than a single molecule can be found within the Rydberg blockade radius r_B , but outside the Rydberg electron orbit radius r_n . Center: Example of interacting channels and potentials involved in the PA process for a given atom-molecule pair (Rb + KRb). The relevant scattering and bound-state wavefunctions are shown. The process efficiency depends on the overlap between the initial scattering state [KRb(0,0)+Rb($5^2S_{1/2}$)] and the final near-threshold vibrational state of the electronically excited trimer [KRb(0,0)+Rb*(n^2L_j)]. The substantial difference of van der Waals lengths between the initial and final states is highlighted. Right: Two-photon scheme for exciting alkali-metal atoms into a target Rydberg state, where atomic states $|g\rangle$, $|e\rangle$, $|r\rangle$ are connected through the lasers ω_1 and ω_2 , giving the two-photon detuning $\delta_\nu = \omega_1 + \omega_2 - (\omega_r - E_\nu)$ from the trimer bound level E_ν . Large intermediate detunings Δ_1 from the excited atomic level prevent gas heating via light scattering.

II. THEORETICAL FRAMEWORK

A. Two photon photoassociation rates

Let us consider a mixed thermal gas consisting of atoms, X, and molecules, AB, in their ground vibrational state. A two-photon excitation resonant with a Rydberg state of the atom, X^* , induces the following light-assisted chemical reaction, known as two-photon photoassociation (PA) [32]:



where X^*-AB represents an excited trimer resonant with an excited electronic state that correlates with the atomic Rydberg state of the atom. These excited states are the long-range van der Waals trimers, and their existence is contingent to the nature of the long-range van der Waals $X^* + AB$ interaction and the reaction rate of Eq. (1).

We consider our atom as $^{85}\text{Rb}(5^2S_{1/2})$ and the molecule, either LiRb or KRb molecules in the ground rovibrational state ($^1\Sigma^+, v = 0, J = 0$) since both of these molecules are available in the cold and ultracold regimes [33–35]. The Rydberg state of the atom is denoted as n^2L_j , where L is the atomic orbital angular momentum and j is the total electronic angular momentum. The initial state of the PA process is a scattering atom+molecule state denoted $|\Psi_l(E_{\text{kin}})\rangle$, with collision energy E_{kin} and partial wave l , in the ground atom-molecule channel [$5^2S_{1/2}|X^1\Sigma^+$]. Here, we assume an s -wave collision between ($l = 0$). The final state of the

process $|\Psi_\nu\rangle$ corresponds to the ν -th bound state of the trimer Rydberg-molecule potential that correlates with the $|n^2L_j\rangle|X^1\Sigma^+$ asymptote. Here, we follow the usual labeling for vibrational states as $\nu = -1, -2, -3, \dots$, where $\nu = -1$ denotes the shallowest bound state.

For distances beyond the Le Roy radius of the Rydberg atom R_{LR} [36], the Rydberg-molecule interaction is given by the van der Waals term $V(r) = -C_6/r^6$, where r is the Rydberg-molecule distance. In many cases, this interaction has been shown to be attractive [37], so it can support bound states depending on the magnitude C_6 . The characterization of the Rydberg-molecular interaction is shown in Figure 2a, displaying the Rydberg-molecule potential depths as a function of the atomic main quantum number n for all the species being considered. It can be seen that existing bound states energies range between 0.2 kHz to 2 MHz. We computed the number of bound states for each species using the Wentzel–Kramers–Brillouin (WKB) approximation, and the results agree with exact numerical calculations as shown in panels (b) and (c) of Figure 2. Highly excited n -states have a larger Le Roy radius, which reduces the effective range of the attractive van der Waals force. As a result, the potential well becomes shallower, limiting the number of bound states. The C_6 coefficient, which depends on the molecular structure, is an order of magnitude larger for LiRb than for KRb, explaining the observed difference in the number of bound states [38]

We compute PA rates for $15 \leq n \leq 50$ Rydberg levels in the $^2S_{1/2}$ and $^2D_{3/2}$ atomic channels, but the formalism can be equally applied to other atomic and molecu-

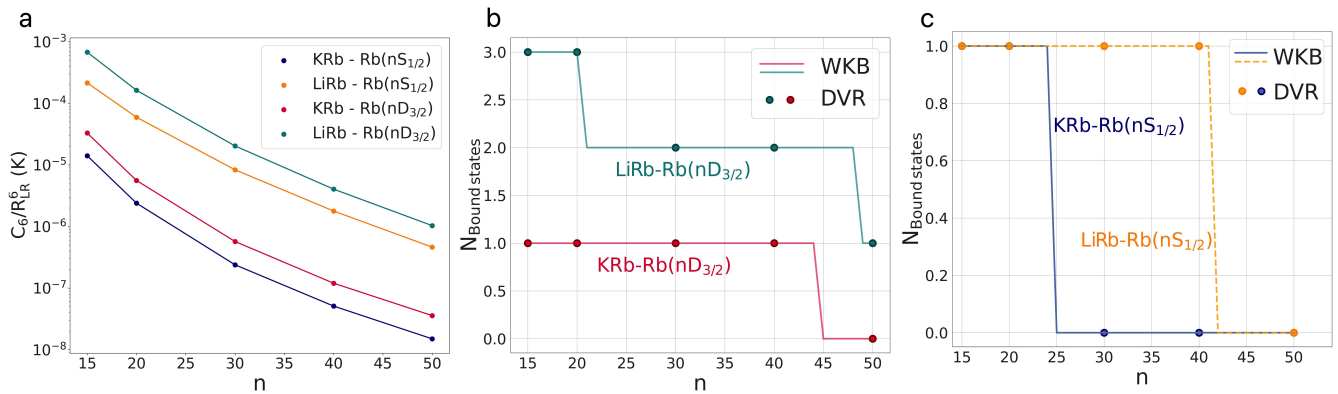


FIG. 2: **Characterization of the long-range Rydberg-molecule energy landscape.** Panel (a) shows the dissociation energy of the trimer, it means, the Van der Waals potential evaluated at the minimum distance R_{LR} . Panels (b) and (c) presents the number of bound states of each Rydberg-molecule potential, for the D and S states respectively. Both panels show the results as a function of the principal quantum number and the species considered.

lar states, provided the C_6 coefficients in the initial and final states are known. From resonance scattering theory [32, 39], the PA rate constant can be written as

$$K_{PA}(E_{\text{kin}}) = v_{\text{rel}} \frac{\pi}{k^2} \sum_{l=0}^{\infty} (2l+1) |S_{\nu}(E_{\text{kin}}, l)|^2, \quad (2)$$

where $v_{\text{rel}} = \sqrt{8k_B T / \pi \mu}$ is the relative velocity of the particles in the entrance channel, μ is the reduced mass of the Rydberg atom-molecule system, and $k = \sqrt{2\mu k_B T / \hbar^2}$ is the channel wavevector. k_B is the Boltzmann's constant and T is the temperature. The rate constant is determined by the element of S -matrix that connects the scattering state and the bound state, given by [32]

$$|S_{\nu}(E_{\text{kin}}, l)|^2 = \frac{\gamma \Gamma_{\nu}(E_{\text{kin}}, l)}{[E_{\text{kin}}/\hbar + \delta_{\nu}]^2 + [\Gamma_T/2]^2}, \quad (3)$$

where $\delta_{\nu} = \omega_1 + \omega_2 - (E_a - E_{\nu})$ is the two-photon detuning from the final state $|\Psi_{\nu}\rangle$, where E_a is the energy of the $\text{Rb}^*(n^2L_j) + \text{Diatom}(X^1\Sigma^+, v=0, J=0)$ asymptote, and E_{ν} is the binding energy of the ν -th near-threshold bound state. We can neglect the possible light-shifts of these resonance frequencies for weak laser dressing fields. The two-photon excitation scheme is further specified in figure 1 (right hand side) in terms of the individual Rabi frequencies Ω_1 and Ω_2 of the driving lasers at ω_1 and ω_2 , respectively. The derivation of the effective two-level approximation used in Eq. (3) is given in the appendix A.

The width of the scattering resonance in Eq.(3) depends on the overall decay rate of the atom-molecule trimer state, given by $\Gamma_T = \gamma + \Gamma_{\nu}(E_{\text{kin}}, l)$, where γ is the natural linewidth of the Rydberg state and the stimulated absorption rate is given by

$$\Gamma_{\nu}(E_{\text{kin}}, l) = 2\pi |V_{\nu}(E_{\text{kin}}, l)|^2, \quad (4)$$

where

$$V_{\nu}(E_{\text{kin}}, l) = \frac{\Omega_{\text{eff}}}{2} \langle \Psi_{\nu} | \Psi_l(E_{\text{kin}}) \rangle. \quad (5)$$

Here, $\langle \Psi_{\nu} | \Psi_l(E_{\text{kin}}) \rangle$ represent the Franck-Condon Factor (FCF) between the initial scattering wavefunction and the final bound state wavefunction. For loosely bound vibrational states, it is a good approximation to neglect the radial dependence of the electric transition dipole moment, leading to an effective two-photon Rabi frequency as $\Omega_{\text{eff}} = \Omega_1 \Omega_2 / 2\Delta_1$ (more details in Ref. [40] and in the appendix A).

The bound state trimer wavefunctions were computed using the mapped Fourier Grid Hamiltonian method [41] and the initial scattering wavefunction via the Numerov method. With this information at hand, we compute the stimulated absorption coefficients for $\text{LiRb-Rb}^*(15 D_{3/2})$ and $\text{LiRb-Rb}^*(20 D_{3/2})$.

B. Scattering and bound state wavefunctions

The initial scattering wavefunction was obtained by solving numerically the Schrödinger equation describing the interaction of ground state LiRb(KRb) with ground states Rb . We solve the radial equation with the Numerov method assuming a Lennard-Jones potential between the atom and the molecule. For LiRb interacting with Rb the Lennard-Jones parameters are $C_6 = 7159$ a.u., $D_e = 2036 \text{ cm}^{-1}$ and $C_{12} = C_6^2/4D_e$, while for KRb interacting with Rb we have $C_6 = 8798$ a.u., $D_e = 1584 \text{ cm}^{-1}$, with the same definition for C_{12} . Both set of parameters are taken from Ref. [42].

Bound state wavefunctions $|\Psi_{\nu}\rangle$ are calculated using a mapped Fourier grid Hamiltonian method [41] given an Rydberg-molecule effective trimer potential. It was mention that the potential follows the Van der Waals expression $V(R) = C_6/R^6$ up to $R = R_c$ where we impose a

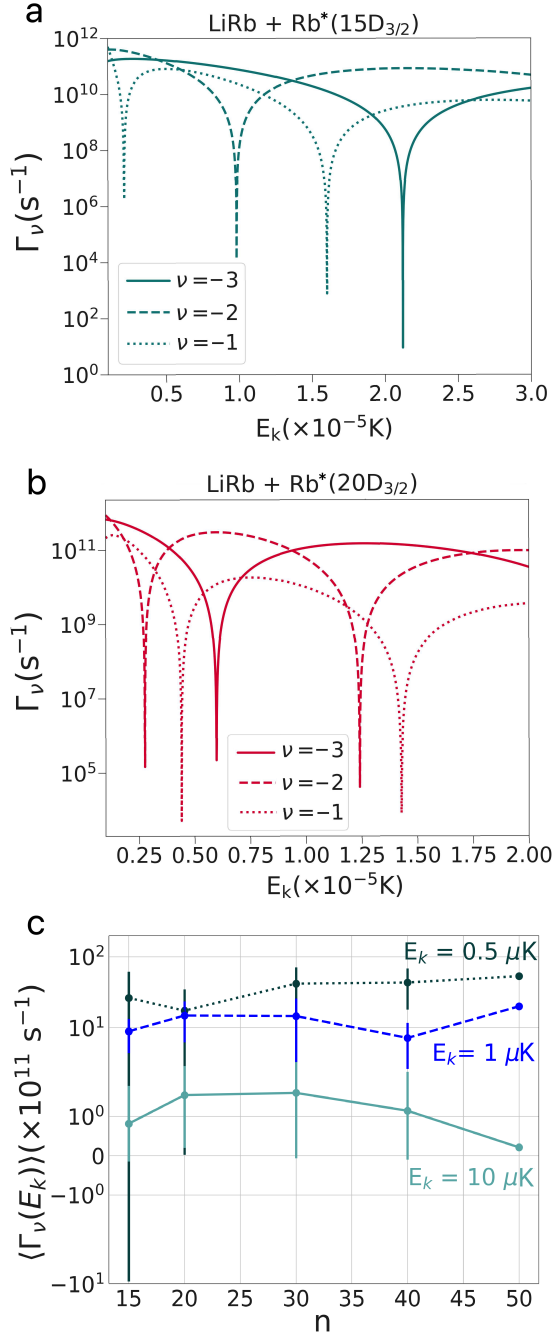


FIG. 3: **Stimulated Absorption rates as a function of the kinetic energy of the (LiRb + Rb*) collision pair** Panel (a) presents the stimulated absorption rates for Rb*(15D_{3/2}). Rydberg state, equivalently for Panel (b) showing the Rb*(20D_{3/2}) state. Panel (c) is the average, over available bound states, absorption rate as a function of the principal quantum number n for LiRb+Rb*(n D_{3/2}) at different collision energies.

repulsive barrier avoiding further penetration. The discussed results were obtained using $R_c = 1.1R_{LR}$, where the Le Roy radius is estimated from $R_{LR} \sim \sqrt{10}n^2a_0$. The convergence of the results was tested by varying the position of the barrier between R_{LR} and $1.2 R_{LR}$. The relative deviation in the energy of threshold states, which are the most affected by the barrier position, ranges from 9% - 16%, scaling with the value of the Le Roy radius. Additionally, even without knowing the exact barrier position, we can confirm that the energy of the threshold bound state does not exceed the theoretical limit $E_{-1} \approx 39.5 E_{vdW}$ in the s -wave regime as outlined in ref. [43]. Here, $E_{vdW} \equiv \sqrt{2}\hbar^3/\mu^{3/2}C_6^{1/2}$. As a specific example, for the highly excited LiRb+Rb*(50D_{3/2}) state, the theoretical threshold-state energy is approximately 1.694×10^{-2} MHz, while the reported value we used is 1.062×10^{-2} MHz. The remaining bound states are generally farther from their respective theoretical limits. The obtained number of bound states coincides with analytical estimates from the WKB approximation which yields, for a given C_6 coefficient, a total number of bound states $N_{max} = \frac{1}{10n^4} \sqrt{\frac{\mu C_6}{2\pi^2}} + \frac{\pi}{4}$. Where the outer turning point is approximated to be at $R = \infty$ and the inner one at $R = R_{LR}$, to perform the integral.

III. RESULTS

The results are shown in figure 3 assuming the following Rydberg dressing parameters: $\Delta_1 = 80$ MHz, $\Omega_1 = 10$ MHz and $\Omega_2 = 8$ MHz, corresponding to laser intensities $I_1 = 10^{-4}$ W/cm² and $I_2 = 1.5$ W/cm² at frequencies ω_1 and ω_2 , respectively. The stimulated absorption rates are rather smooth except for certain dips. These are due to the energy-dependent oscillatory nature of the continuum wavefunction that affects its overlap with a given bound wavefunction. The average, with respect to all available bound states, stimulated absorption rate for LiRb+Rb*(n D_{3/2}), on the other hand, shows a weak dependence with the principal quantum number independently of the collision energy. However, at lower collision energies, the rate is systematically larger than that of higher collision energies. Therefore, the observation of the Van der Waals trimer states will benefit from colder temperatures.

We compute the two-photon PA lineshape profile for the LiRb-Rb(15 D_{3/2}), and the results are shown in figure 4. This figure displays the PA rate as a function of the two-photon detuning with respect to the least bound state associated with the LiRb-Rb(15 D_{3/2}) asymptote. The spectral overlap closely resembles the Lorentzian profile from equation 3 due to the low energy values of the bound states relative to the kinetic energy. This causes all peaks to appear tightly centered around $\delta_\nu = 0$. However, a closer examination of the spectrum, as shown in panel (b), reveals a more intricate structure where each bound state contributes uniquely. It is important to note that

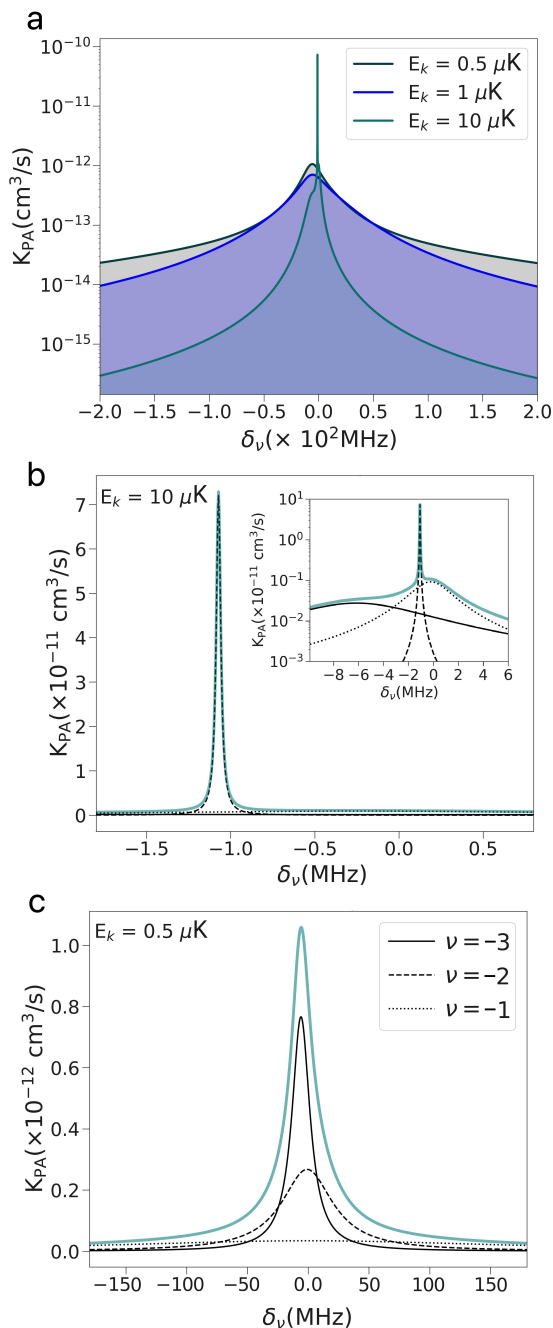


FIG. 4: **Photoassociation lineshape for LiRb+Rb*(15 D_{3/2}) for different collision energies.** Panel (a) shows the PA lineshape for three collision energies. Panels (b) and (c) are the K_{PA} constants for $E_{kin} = 10 \mu\text{K}$ and 500 nK , respectively, including the contributions from each vibrational state. The inset on panel (b) is a zoom-in of the PA peak. The color coding for panels (b) and (c) is the same: vibrational states are given in panel (c), and the total spectrum is in cyan.

the peak intensity of each contribution varies with the collision energy. The width of the PA spectra shows the expected inverse proportionality of the spectrum broadening with the temperature, as in figure 4.a .

Finally, we report the PA rate peak for four different Rydberg-molecule combinations as a function of the principal quantum number, and the results are shown in figure 5. Independently of the species under consideration, the peak PA rate varies from 10^{-13} - $10^{-11} \text{ cm}^3 \text{ s}^{-1}$. Clearly, systems involving Rydberg atoms in the D state outperform those with a Rydberg in the S state since the former shows larger C_6 coefficients. It seems that low principal quantum number states favor the PA rate toward the formation of long-range van der Waals Rydberg trimers, which arises from the dependence of the S-matrix elements on the bound state energies and the Franck-Condon factors (equation 3). The absence of bound states for sufficiently large n values (Figure 2) is consistent with previous observations in the $\text{Rb}^* + \text{KRb}$ system, in the context of inner-orbital long-range Rydberg trimers [27].

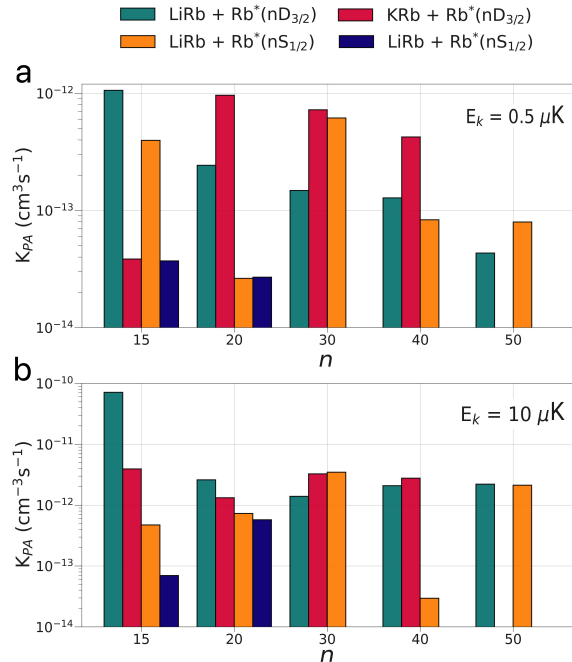


FIG. 5: **Peak photoassociation rates constant for LiRb-Rb* and KRb-Rb*.** Panels (a) and (b) displays the peak PA rate constants assuming a collision energy of 500 nK and $10 \mu\text{K}$, respectively.

IV. CONCLUSIONS

We predict that long-range van der Waals Rydberg trimers exists in nature. The extension of these exotic trimers spans from 5 to 500 nm, depending on the atomic principal quantum number n and orbital quan-

tum number L . The size is comparable to other exotic Rydberg molecules such as trilobite and butterfly [9, 11, 12, 14, 15, 44]. Using the width of the PA absorption spectrum, We estimate the lifetime of the trimer states to range from 10^{-9} to 10^{-4} s, indicating that they could be synthesized in the lab via two photon PA.

To discuss the feasibility of observing these new exotic Rydberg molecules, first, we consider the stimulated absorption rate, which in our case is $\sim 10^{12}\text{s}^{-1}$. This number should be compared with PA rates measured for the formation of alkali-metal dimers from weakly excited (low n) alkali metal atoms. Experiments at $100\ \mu\text{K}$ have measured stimulated rates of $1.5 \times 10^8\ \text{s}^{-1}$ for RbCs [45] and $3.5 \times 10^7\ \text{s}^{-1}$ for LiRb [33], using PA laser intensities of the order of 10^2 – $10^3\ \text{W}/\text{cm}^2$. These examples involve species that interact also via van der Waals forces, but with values of C_6 that are several orders of magnitude smaller than our case. In addition, the PA process in these bi-alkali systems occurs at relative short distances [32], which makes the process more sensitive to the details of the initial scattering wavefunction. Therefore, the predicted stimulated absorption rate is indicative that the photoassociation between a Rydberg atom and a diatomic polar molecule into a long-range van der Waals Rydberg molecule is somewhat efficient.

To observe long-range van der Waals Rydberg trimers, we propose to work on a regime where the molecular density is much smaller than the density of Rydberg atoms. We estimate the latter by requiring that at most one molecule resides within the Rydberg blockade radius r_B , which depends on the van der Waals interaction between atoms in identical Rydberg levels [2]. Given a laser-dependent Rydberg excitation fraction $f < 1$, the critical ground atom density ρ_B below which we can ignore blockade effects can be estimated from $f \times \rho_B \times (4/3)\pi r_B^3 = 1$ [1]. Assuming weak dressing $f \sim 10^{-2}$ and $r_B \sim 1\ \mu\text{m}$ [46], the relevant atom densities for this work $\rho_B \sim 10^{10}\ \text{cm}^{-3}$ are thus compatible with magneto-optical trapping [47, 48].

In comparison with traditional cold-molecule formation experiments that target high-density molecular ensembles [49], our Rydberg trimer predictions could be tested in a low-density regime where independent molecules are diluted in a background gas of alkali-metal atoms for atomic densities below the critical value beyond which Rydberg blockade effects become important [50]. On the other hand, ultra-long-range van der Waals Rydberg trimers could be synthesized using optical tweezers. In this scenario, the molecule and atom are in adjacent tweezers and the atom in the next one, so the two-photon photoassociation profile is considered a function of the distance between the two tweezer traps. Thus, our work sets the foundations for a deeper understanding of the exotic properties of ultracold molecules in atomic Rydberg reservoirs.

V. ACKNOWLEDGMENTS

M.L.C. and J.P.-R. acknowledge the support from the Stony Brook OVPR seed program and the the Simons Foundation. F.H. and V.O.-A. were supported by ANID through grants Fondecyt Regular 1221420 and Millennium Scientific Initiative ICN17_012.

Appendix A: Effective two-level system

The Hamiltonian that describes a three-level system as the one shown in Figure 1 is given by ($\hbar = 1$)

$$H = \omega_e |e\rangle\langle e| + \omega_r |r\rangle\langle r| + \frac{\Omega_1}{2} [|g\rangle\langle e|e^{i\omega_1 t} + |e\rangle\langle g|e^{-i\omega_1 t}] + \frac{\Omega_2}{2} [|e\rangle\langle r|e^{i\omega_2 t} + |r\rangle\langle e|e^{-i\omega_2 t}], \quad (\text{A1})$$

where ω_e (ω_r) is the energy of the $|e\rangle$ ($|r\rangle$) state and the energy of $|g\rangle$ is set to zero. Ω_a and ω_a are the Rabi frequency and energy of the laser a , with $a = 1, 2$.

Using an unitary rotation frame transformation $U(t) = |g\rangle\langle g| + e^{i\omega_1 t}|e\rangle\langle e| + e^{i(\omega_1 + \omega_2)t}|r\rangle\langle r|$, the interaction Hamiltonian can be written as [51]

$$H_I = -\Delta_1 |e\rangle\langle e| + \delta |r\rangle\langle r| + \frac{\Omega_1}{2} [|g\rangle\langle e| + |e\rangle\langle g|] + \frac{\Omega_2}{2} [|e\rangle\langle r| + |r\rangle\langle e|], \quad (\text{A2})$$

where $\delta = \omega_r - (\omega_1 + \omega_2)$ and $\Delta_1 = \omega_1 - \omega_e$. The time evolution of the system is determined by the Schrödinger equation $i\partial_t|\Psi\rangle = H_I|\Psi\rangle$, where $|\Psi(t)\rangle = c_g(t)|g\rangle + c_e(t)|e\rangle + c_r(t)|r\rangle$ is the system state. In the rotating frame, $|e\rangle$ has fast oscillations and this state instantaneously tends to a steady state compared with the slow motion of the rest of the system, therefore we assume that $\dot{c}_e = 0$. Thus, the equations of motion are given by

$$i\dot{c}_g(t) = \frac{\Omega_1^2}{4\Delta_1} c_g(t) + \frac{\Omega_1\Omega_2}{4\Delta_1} c_r(t), \quad (\text{A3})$$

$$i\dot{c}_r(t) = \delta c_r(t) + \frac{\Omega_2^2}{4\Delta_1} c_r(t) + \frac{\Omega_1\Omega_2}{4\Delta_1} c_g(t). \quad (\text{A4})$$

Eqs. (A3) and (A4) are the same differential equation obtained from a two-level system with an effective Rabi frequency $\Omega_{\text{eff}} = \frac{\Omega_1\Omega_2}{2\Delta_1}$ and an effective detuning

$$\delta_{\text{eff}} = \delta + \frac{\Omega_2^2}{4\Delta_1} - \frac{\Omega_1^2}{4\Delta_1}. \quad (\text{A5})$$

TABLE I: Total PA rate constant peak for the Dimer+nD_{3/2}(Rb) at different temperatures. The rate peak is expressed in cm³/s⁻¹

Molecule	n	Vibrational energy (MHz)	$E_k = 0.5 \mu\text{K}$	$E_k = 1 \mu\text{K}$	$E_k = 10 \mu\text{K}$
	15	$\nu_{-3} = 6.049$ $\nu_{-2} = 8.783 \times 10^{-1}$ $\nu_{-1} = 3.916 \times 10^{-3}$	1.06×10^{-12}	6.98×10^{-13}	7.12×10^{-11}
	20	$\nu_{-3} = 1.671$ $\nu_{-2} = 2.347 \times 10^{-1}$ $\nu_{-1} = 1.492 \times 10^{-3}$	2.43×10^{-13}	4.79×10^{-13}	2.60×10^{-12}
LiRb	30	$\nu_{-2} = 1.341 \times 10^{-1}$ $\nu_{-1} = 2.404 \times 10^{-3}$	1.48×10^{-13}	3.12×10^{-13}	1.39×10^{-12}
	40	$\nu_{-2} = 6.036 \times 10^{-2}$ $\nu_{-1} = 2.301 \times 10^{-3}$	1.28×10^{-13}	5.70×10^{-13}	2.08×10^{-12}
	50	$\nu_{-1} = 1.061 \times 10^{-2}$	4.33×10^{-14}	3.00×10^{-12}	2.21×10^{-12}
	15	$\nu_{-1} = 2.741 \times 10^{-2}$	3.85×10^{-14}	4.14×10^{-14}	3.92×10^{-12}
KRb	20	$\nu_{-1} = 2.808 \times 10^{-3}$	9.62×10^{-13}	1.11×10^{-13}	1.32×10^{-12}
	30	$\nu_{-1} = 2.201 \times 10^{-3}$	7.23×10^{-13}	3.92×10^{-13}	2.25×10^{-12}
	40	$\nu_{-1} = 1.370 \times 10^{-3}$	4.24×10^{-13}	1.59×10^{-13}	2.77×10^{-12}

TABLE II: Total PA rate constant peak for the Dimer+nS_{1/2}(Rb) at different temperatures. The rate peak is expressed in cm³/s⁻¹

Molecule	n	Vibrational energy (MHz)	$E_k = 0.5 \mu\text{K}$	$E_k = 1 \mu\text{K}$	$E_k = 10 \mu\text{K}$
	15	$\nu_{-2} = 1.257$ $\nu_{-1} = 1.229 \times 10^{-3}$	3.96×10^{-13}	3.94×10^{-13}	4.72×10^{-13}
	20	$\nu_{-1} = 9.152 \times 10^{-3}$	2.63×10^{-14}	6.97×10^{-14}	7.38×10^{-13}
LiRb	30	$\nu_{-1} = 2.128 \times 10^{-3}$	6.15×10^{-13}	3.25×10^{-13}	3.47×10^{-12}
	40	$\nu_1 = 1.396 \times 10^{-3}$	8.31×10^{-14}	4.83×10^{-12}	2.95×10^{-14}
	50	$\nu_{-1} = 2.079 \times 10^{-4}$	7.96×10^{-14}	1.35×10^{-13}	2.12×10^{-12}
	15	$\nu_{-1} = 2.132 \times 10^{-2}$	3.71×10^{-14}	7.30×10^{-14}	6.95×10^{-14}
KRb	20	$\nu_{-1} = 1.157 \times 10^{-3}$	2.69×10^{-14}	4.67×10^{-14}	5.74×10^{-13}

- [1] T. F. Gallagher, *Rydberg atoms*, 3 (Cambridge University Press, 2005).
- [2] M. Saffman, T. G. Walker, and K. Mølmer, Quantum information with rydberg atoms, *Rev. Mod. Phys.* **82**, 2313 (2010).
- [3] A. Browaeys and T. Lahaye, Many-body physics with individually controlled rydberg atoms, *Nature Physics* **16**,

132 (2020).

- [4] M. Schlagmüller, T. C. Liebisch, F. Engel, K. S. Kleinbach, F. Böttcher, U. Hermann, K. M. Westphal, A. Gaj, R. Löw, S. Hofferberth, T. Pfau, J. Pérez-Ríos, and C. H. Greene, Ultracold chemical reactions of a single Rydberg atom in a dense gas, *Phys. Rev. X* **6**, 031020 (2016).
- [5] J. Pérez-Ríos, *An Introduction to Cold and Ultracold*

- Chemistry* (Springer International Publishing, 2020).
- [6] T. Karman, M. Tomza, and J. Pérez-Ríos, Ultracold chemistry as a testbed for few-body physics, *Nature Physics* **20**, 722 (2024).
- [7] T. C. Liebisch, M. Schlagmüller, F. Engel, H. Nguyen, J. Balewski, G. Lochead, F. Böttcher, K. M. Westphal, K. S. Kleinbach, T. Schmid, A. Gaj, R. Löw, S. Hofferberth, T. Pfau, J. Pérez-Ríos, and C. H. Greene, Controlling rydberg atom excitations in dense background gases, *Journal of Physics B: Atomic, Molecular and Optical Physics* **49**, 182001 (2016).
- [8] T. Scheuing and J. Pérez-Ríos, Quasi-static lineshape theory for rydberg excitations in high-density media, *Atoms* **11**, 10.3390/atoms11060095 (2023).
- [9] C. H. Greene, A. S. Dickinson, and H. R. Sadeghpour, Creation of polar and nonpolar ultra-long-range rydberg molecules, *Phys. Rev. Lett.* **85**, 2458 (2000).
- [10] V. Bendkowsky, B. Butscher, J. Nipper, J. P. Shaffer, R. Löw, and T. Pfau, Observation of ultralong-range rydberg molecules, *Nature* **458**, 1005 (2009).
- [11] E. L. Hamilton, C. H. Greene, and H. R. Sadeghpour, Shape-resonance-induced long-range molecular rydberg states, *Journal of Physics B: Atomic, Molecular and Optical Physics* **35**, L199 (2002).
- [12] A. A. Khuskivadze, M. I. Chibisov, and I. I. Fabrikant, Adiabatic energy levels and electric dipole moments of rydberg states of Rb_2 and Cs_2 dimers, *Phys. Rev. A* **66**, 042709 (2002).
- [13] A. Gaj, A. T. Krupp, J. B. Balewski, R. Löw, S. Hofferberth, and T. Pfau, From molecular spectra to a density shift in dense rydberg gases, *Nature Communications* **5**, 4546 (2014).
- [14] D. Booth, S. T. Rittenhouse, J. Yang, H. R. Sadeghpour, and J. P. Shaffer, Production of trilobite rydberg molecule dimers with kilo-debye permanent electric dipole moments, *Science* **348**, 99 (2015), <https://science.sciencemag.org/content/348/6230/99.full.pdf>
- [15] T. Niederprüm, O. Thomas, T. Eichert, C. Lippe, J. Pérez-Ríos, C. H. Greene, and H. Ott, Observation of pendular butterfly rydberg molecules, *Nature Communications* **7**, 12820 (2016).
- [16] C. Fey, F. Hummel, and P. Schmelcher, Ultralong-range rydberg molecules, *Molecular Physics* **118**, e1679401 (2020), <https://doi.org/10.1080/00268976.2019.1679401>.
- [17] V. Bendkowsky, B. Butscher, J. Nipper, J. P. Shaffer, R. Löw, and T. Pfau, Observation of ultralong-range rydberg molecules, *Nature* **458**, 1005 (2009).
- [18] J. P. Shaffer, S. T. Rittenhouse, and H. R. Sadeghpour, Ultracold rydberg molecules, *Nature Communications* **9**, 1965 (2018).
- [19] M. T. Eiles, J. Pérez-Ríos, F. Robicheaux, and C. H. Greene, Ultracold molecular rydberg physics in a high density environment, *Journal of Physics B: Atomic, Molecular and Optical Physics* **49**, 114005 (2016).
- [20] F. Camargo, R. Schmidt, J. D. Whalen, R. Ding, G. Woehl, S. Yoshida, J. Burgdörfer, F. B. Dunning, H. R. Sadeghpour, E. Demler, and T. C. Killian, Creation of Rydberg polarons in a Bose gas, *Phys. Rev. Lett.* **120**, 083401 (2018).
- [21] J. Sous, H. R. Sadeghpour, T. C. Killian, E. Demler, and R. Schmidt, Rydberg impurity in a Fermi gas: Quantum statistics and rotational blockade, *Phys. Rev. Research* **2**, 023021 (2020).
- [22] A. A. T. Durst and M. T. Eiles, Phenomenology of a rydberg impurity in an ideal bose-einstein condensate, *Phys. Rev. Res.* **6**, L042009 (2024).
- [23] N. Bigagli, W. Yuan, S. Zhang, B. Bulatovic, T. Karman, I. Stevenson, and S. Will, Observation of bose-einstein condensation of dipolar molecules., *Nature* (2023).
- [24] S. L. Cornish, M. R. Tarbutt, and K. R. A. Hazzard, Quantum computation and quantum simulation with ultracold molecules, *Nature Phys.* **20**, 730 (2024), arXiv:2401.05086 [cond-mat.quant-gas].
- [25] T. Langen, J. Boronat, J. Sánchez-Baena, R. Bombín, T. Karman, and F. Mazzanti, Dipolar droplets of strongly interacting molecules, arXiv e-prints , arXiv:2407.09391 (2024), arXiv:2407.09391 [cond-mat.quant-gas].
- [26] M. Wenzel, T. Pfau, and I. Ferrier-Barbut, A fermionic impurity in a dipolar quantum droplet, *Physica Scripta* **93**, 104004 (2018).
- [27] J. Aguilera-Fernández, H. R. Sadeghpour, P. Schmelcher, and R. González-Férez, Electronic structure of ultralong-range rydberg penta-atomic molecules with two polar diatomic molecules, *Phys. Rev. A* **96**, 052509 (2017).
- [28] R. González-Férez, S. T. Rittenhouse, P. Schmelcher, and H. R. Sadeghpour, Rydberg polyatomic molecules: Electronic structure and experimental proposal for their creation, *Journal of Physics: Conference Series* **1412**, 122002 (2020).
- [29] R. González-Férez, J. Shertzer, and H. R. Sadeghpour, Ultralong-range rydberg bimolecules, *Phys. Rev. Lett.* **126**, 043401 (2021).
- [30] C. Zhang, S. T. Rittenhouse, T. V. Tscherbul, H. R. Sadeghpour, and N. R. Hutzler, Sympathetic cooling and slowing of molecules with rydberg atoms, *Phys. Rev. Lett.* **132**, 033001 (2024).
- [31] D. Mellado-Alcedo, A. Guttridge, S. L. Cornish, H. R. Sadeghpour, and R. González-Férez, Ultralong-range CsRbCs rydberg molecules: Nonadiabaticity of dipole moments, *Phys. Rev. A* **110**, 013314 (2024).
- [32] K. M. Jones, E. Tiesinga, P. D. Lett, and P. S. Julienne, Ultracold photoassociation spectroscopy: Long-range molecules and atomic scattering, *Rev. Mod. Phys.* **78**, 483 (2006).
- [33] S. Dutta, J. Lorenz, A. Altaf, D. S. Elliott, and Y. P. Chen, Photoassociation of ultracold LiRb^* molecules: Observation of high efficiency and unitarity-limited rate saturation, *Phys. Rev. A* **89**, 020702 (2014).
- [34] D. B. Blasing, I. C. Stevenson, J. Pérez-Ríos, D. S. Elliott, and Y. P. Chen, Short-range photoassociation of LiRb , *Phys. Rev. A* **94**, 062504 (2016).
- [35] K.-K. Ni, S. Ospelkaus, M. H. G. de Miranda, A. Pe'er, B. Neyenhuis, J. J. Zirbel, S. Kotochigova, P. S. Julienne, D. S. Jin, and J. Ye, A high phase-space-density gas of polar molecules, *Science* **322**, 231 (2008), <https://www.science.org/doi/pdf/10.1126/science.1163861>.
- [36] R. J. Le Roy, Theory of deviations from the limiting near-dissociation behavior of diatomic molecules, *The Journal of Chemical Physics* **73**, 6003 (1980), <https://doi.org/10.1063/1.440134>.
- [37] V. Olaya, J. Pérez-Ríos, and F. Herrera, C_6 coefficients for interacting rydberg atoms and alkali-metal dimers, *Phys. Rev. A* **101**, 032705 (2020).
- [38] For example, for $\text{Rb}^*(15D_{1/2})$, the van der Waals coefficients are $C_6(\text{LiRb}) = -2.778 \times 10^8$ a.u., and $C_6(\text{KRb}) = -1.351 \times 10^7$ a.u. The Le Roy radius is the same in both cases, approximately $712 a_0$.

- [39] J. L. Bohn and P. S. Julienne, Semianalytic theory of laser-assisted resonant cold collisions, *Phys. Rev. A* **60**, 414 (1999).
- [40] A. Browaeys, D. Barredo, and T. Lahaye, Experimental investigations of dipole–dipole interactions between a few rydberg atoms, *Journal of Physics B: Atomic, Molecular and Optical Physics* **49**, 152001 (2016).
- [41] V. Kokoouline, O. Dulieu, R. Kosloff, and F. Masnou-Seeuws, Mapped fourier methods for long-range molecules: Application to perturbations in the rb2(0u+) photoassociation spectrum, *The Journal of Chemical Physics* **110**, 9865 (1999), <https://doi.org/10.1063/1.478860>.
- [42] M. Mayle, B. P. Ruzic, and J. L. Bohn, Statistical aspects of ultracold resonant scattering, *Phys. Rev. A* **85**, 062712 (2012).
- [43] B. Gao, Zero-energy bound or quasibound states and their implications for diatomic systems with an asymptotic van der waals interaction, *Phys. Rev. A* **62**, 050702 (2000).
- [44] P. Giannakeas, M. T. Eiles, F. Robicheaux, and J. M. Rost, Dressed ion-pair states of an ultralong-range rydberg molecule, *Phys. Rev. Lett.* **125**, 123401 (2020).
- [45] A. J. Kerman, J. M. Sage, S. Sainis, T. Bergeman, and D. DeMille, Production of ultracold, polar rbc* molecules via photoassociation, *Phys. Rev. Lett.* **92**, 033004 (2004).
- [46] K. Singer, J. Stanojevic, M. Weidemüller, and R. Côté, Long-range interactions between alkali rydberg atom pairs correlated to thens–ns,np–np andnd–nd asymptotes, *Journal of Physics B: Atomic, Molecular and Optical Physics* **38**, S295 (2005).
- [47] K. Singer, M. Reetz-Lamour, T. Amthor, L. G. Marcassa, and M. Weidemüller, Suppression of excitation and spectral broadening induced by interactions in a cold gas of rydberg atoms, *Phys. Rev. Lett.* **93**, 163001 (2004).
- [48] D. Tong, S. M. Farooqi, J. Stanojevic, S. Krishnan, Y. P. Zhang, R. Côté, E. E. Eyler, and P. L. Gould, Local blockade of rydberg excitation in an ultracold gas, *Phys. Rev. Lett.* **93**, 063001 (2004).
- [49] K. Matsuda, L. D. Marco, J.-R. Li, W. G. Tobias, G. Valtolina, G. Quémener, and J. Ye, Resonant collisional shielding of reactive molecules using electric fields, *Science* **370**, 1324 (2020), <https://www.science.org/doi/pdf/10.1126/science.abe7370>.
- [50] J. B. Balewski, A. T. Krupp, A. Gaj, S. Hofferberth, R. Löw, and T. Pfau, Rydberg dressing: understanding of collective many-body effects and implications for experiments, *New Journal of Physics* **16**, 063012 (2014).
- [51] D. A. Steck, *Quantum and Atom Optics* (Available online at <http://steck.us/teaching>, revision 0.13.4, 24 September 2020).